OPEN ACCESS
IOP Publishing
Semiconductor Science and Technology
Semicond. Sci. Technol. **34** (2019) 035032 (7pp)
https://doi.org/10.1088/1361-6641/ab0331

Effect of HCl cleaning on InSb–Al_2O_3 MOS capacitors

Oliver J Vavasour[1], Richard Jefferies[1], Marc Walker[2], Joseph W Roberts[3], Naomi R Meakin[1], Peter M Gammon[1], Paul R Chalker[3] and Tim Ashley[1]

[1] School of Engineering, University of Warwick, Coventry CV4 7AL, United Kingdom
[2] Department of Physics, University of Warwick, Coventry CV4 7AL, United Kingdom
[3] School of Engineering, University of Liverpool, Liverpool, L69 3GH, United Kingdom

E-mail: o.vavasour@warwick.ac.uk

Received 6 November 2018, revised 21 January 2019
Accepted for publication 30 January 2019
Published 26 February 2019

Abstract

In this work, the role of HCl treatments on InSb surfaces and InSb–Al_2O_3 dielectric interfaces is characterised. X-ray photoelectron spectroscopy measurements indicate that HCl diluted in and rinsed with isopropanol (IPA) results in a surface layer of $InCl_3$ which is not present for similar HCl-water processes. Furthermore, this $InCl_3$ layer desorbs from the surface between 200 °C and 250 °C. Metal–oxide–semiconductor capacitors were fabricated using atomic layer deposition of Al_2O_3 at 200 °C and 250 °C and the presence of $InCl_3$ was associated with a +0.79 V flatband voltage shift. The desorption of the $InCl_3$ layer at 250 °C reversed this shift but the increased process temperature resulted in increased interface-trapped charge (D_{it}) and hysteresis voltage (V_H). This shift in flatband voltage, which does not affect other figures of merit, offers a promising route to manipulate the threshold voltage of MOS transistors, allowing enhancement-mode and depletion-mode devices to be fabricated in parallel.

Keywords: InSb, III–V, HCl, ALD, Al_2O_3, MOSCAP

(Some figures may appear in colour only in the online journal)

1. Introduction

Within the field of semiconductor devices, the III–V material family has presented promising opportunities in a range of engineering applications, most notably optoelectronic devices and high-speed devices. In particular, narrow bandgap semiconductors such as indium arsenide (InAs), gallium antimonide (GaSb) and indium antimonide (InSb) have shown great promise in infrared emitters and detectors [1–4] and ultra-high-speed devices [5, 6]. InSb offers the lowest energy gap of any binary semiconductor and the highest electron mobility and electron saturation velocity of any conventional semiconductor [7, 8]. Fabrication process technology, however, remains deficient in these material systems, with the lack of a suitable surface passivation and dielectric deposition process hindering performance and large-scale adoption of devices. We present a study investigating the role of hydrochloric acid (HCl) solutions on InSb surfaces and dielectric interfaces.

Cleaning of III–V surfaces is critical for the formation of good, defect-free dielectric interfaces. Limited analysis of InSb cleaning has been performed: surface science research has demonstrated vacuum cleaning processes and some metal–oxide–semiconductor structures have been demonstrated in publication. Tereschenko *et al* [9] cleaned InSb surfaces in an inert dry nitrogen atmosphere using a solution of HCl diluted in isopropanol (IPA). When these samples were studied using x-ray photoelectron spectroscopy (XPS), a surface layer of indium chloride ($InCl_3$) was observed. This presents the possibility of using chlorine-based interfacial layers for surface passivation but does not account for oxidation and possible displacement of chlorine in oxygen-containing solutions and atmospheres.

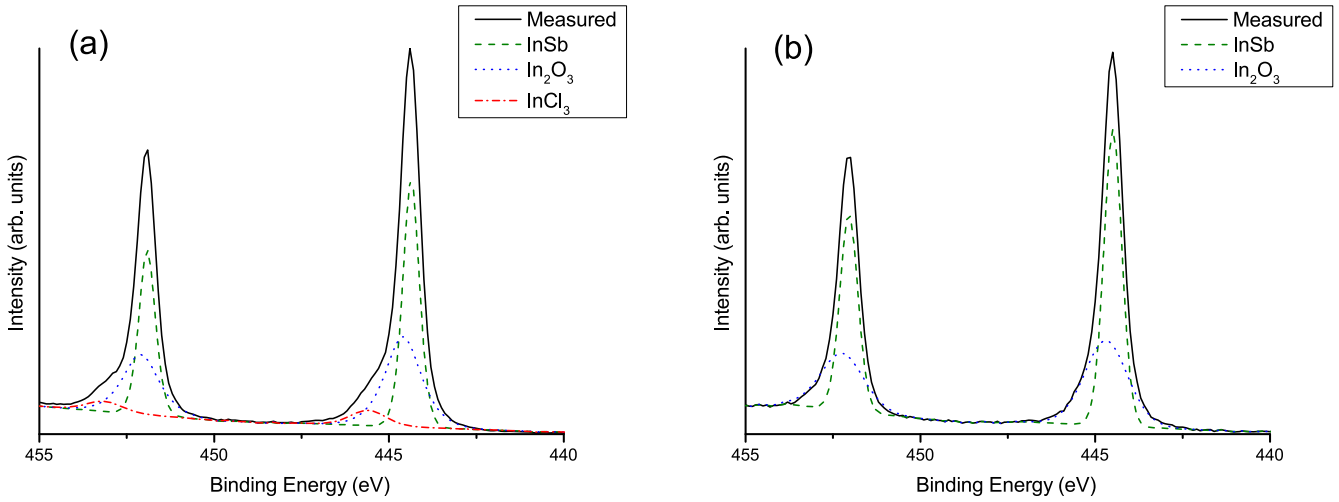

Figure 1. XPS data for the In 3d region of (a) sample A and (b) sample B. The measured data is shown in black, the fitted components for In–Sb, In–O and In–Cl are shown in green, blue and red, respectively.

Table 1. Breakdown of the atomic percentages in each observed bonding environment from the as-loaded surfaces of samples A and B. Values accurate to ±2%.

Sample	Sample A	Sample A	Sample B	Sample B
Component	In $3d_{5/2}$ binding energy (eV)	% of In $3d_{5/2}$ region	In $3d_{5/2}$ binding energy (eV)	% of In $3d_{5/2}$ region
InSb	444.37	51.2	444.49	59.3
In_2O_3	444.60	42.1	444.67	40.7
$InCl_3$	445.60	6.7	N/A	<1

Furthermore, when annealed at 230 °C, the layer was observed to have desorbed from the surface, presenting further questions about the stability of chloride interfacial layers under dielectric deposition conditions. Trinh *et al* [10] fabricated metal–oxide–semiconductor capacitors (MOSCAPs) using InSb substrates, HCl cleaning, atomic layer deposition (ALD) of aluminium oxide (Al_2O_3) and Ni/Au metal and performed capacitance–voltage (C–V) measurements for characterisation. Critically, when the ALD process temperature changed from 200 °C to 250 °C, a small change in flatband voltage was observed which, when accounting for the observations by Tereschenko *et al*, suggests that residual interfacial chlorine may be influencing the electrical characteristics of devices. This behaviour is of particular interest due to the uptake of HCl wet treatments in place of sulphidation treatments, [11–14] necessitating a more complete understanding of how HCl wet treatments influence surfaces and dielectric interfaces. As such, a study has been performed to investigate the role of $InCl_3$ on InSb MOSCAPs, to ascertain whether an $InCl_3$ layer forms under normal processing conditions and whether it survives exposure to ambient oxygen; how quickly it desorbs as the temperature rises through the ALD process temperature window (150 °C–300 °C) and how the MOSCAP electrical behaviour changes as the $InCl_3$ layer is introduced and desorbed.

2. Experimental methodology (XPS)

An XPS study was first performed to investigate the formation and change of $InCl_3$ layers after HCl cleaning. Two samples—1 cm squares of undoped bulk InSb—were prepared and immersed in cleaning solution for 30 s at room temperature, following Tereschenko *et al* [9]. Sample A was cleaned in a 1:5 solution of 37% HCl and IPA and rinsed in IPA and sample B was cleaned in a 1:5 solution of 37% HCl and deionised (DI) water and rinsed in DI water. After cleaning and rinsing, both samples were blow-dried using dry nitrogen and loaded into a vacuum desiccator for transfer to a Kratos Axis Ultra DLD spectrometer for XPS measurements. During this process, the samples were exposed to air for approximately 1 min during loading into the desiccator and 20 s during transfer from the desiccator to the vacuum system —this procedure was used to emulate the total air exposure during transfer in practical fabrication. XPS data were acquired at a take-off angle of 90° with respect to the surface plane at a resolution of approximately 0.4 eV. The samples were illuminated with Al Kα x-rays and the spectrometer work function was calibrated using polycrystalline Ag foil prior to the experiments. XPS data were acquired from the as-loaded surface and following annealing in the chamber for 30 min at 150 °C, 200 °C, 250 °C and 300 °C (temperatures within the ALD window). The data were analysed using the

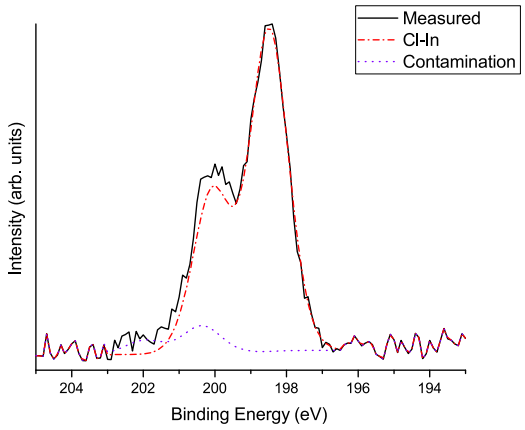

Figure 2. XPS data for the Cl 2p region of sample A. The measured data is shown in black, the fitted components for Cl–In is shown in red and an additional contamination component shown in purple.

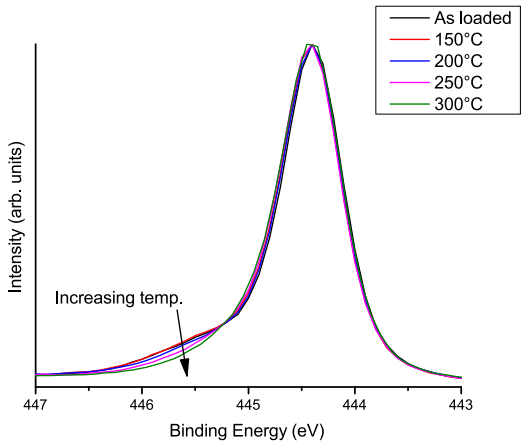

Figure 3. XPS data for the In $3d_{5/2}$ region of sample A. The as-received spectrum is shown in black (top), with spectra after a series of annealing steps shown in colour (below).

CasaXPS software package, employing linear backgrounds and Voigt (Gaussian–Lorentzian) lineshapes.

3. Results and discussion (XPS)

The In 3d spectra acquired from the as-loaded surfaces are shown in figure 1. Both spectra exhibit components at 444.4 eV, assigned to InSb [15, 16] and at 444.6 eV, assigned to In_2O_3 [17–19]. Figure 1(a) shows the spectrum acquired from sample A and exhibits an additional component at 445.6 eV when compared to sample B in figure 1(b), a component attributed to the existence of $InCl_3$ on the surface [20]. Although this component occurs at a relatively low binding energy for In in its +3 oxidation state, as in $InCl_3$, quantitative comparison between In–Cl components from the In 3d and Cl 2p spectra, discussed below and included in table 3, indicate an In:Cl ratio of approximately 1:3, confirming the attribution of $InCl_3$. Table 1 shows a breakdown of the different bonding environments found in the In $3d_{5/2}$ region and reveals that 6.66% of the detected intensity from

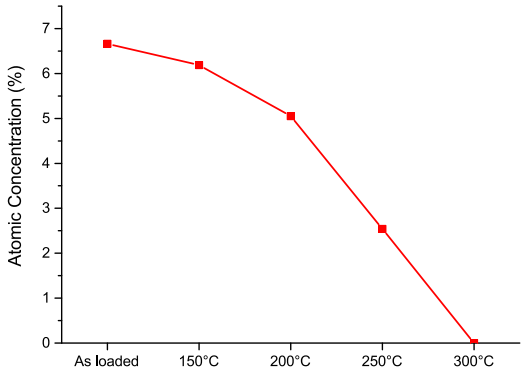

Figure 4. Atomic concentration of $InCl_3$ component relative to total In 3d region as-deposited and after each annealing stage.

Table 2. Breakdown of the atomic percentages in each observed bonding environment (as a percentage of the total In $3d_{5/2}$ region) from sample A as a function of annealing temperature. Values accurate to ±2%.

Component	As-loaded	150 °C	200 °C	250 °C	300 °C
InSb	51.2	51.4	52.1	53.5	54.8
In_2O_3	42.1	42.4	42.9	44.0	45.2
$InCl_3$	6.7	6.2	5.0	2.5	<1

sample A was due to $InCl_3$. The absence of $InCl_3$ in sample B is due to the increased solubility of $InCl_3$ in water compared to IPA.

To further corroborate the existence of the $InCl_3$ layer, the Cl 2p spectrum from sample A is shown in figure 2 (no Cl 2p photoemission is observed from sample B). The spectrum shows two pairs of components, with the Cl $2p_{3/2}$ peak of the main pair found to be at 198.48 eV, corresponding well with the expected energy for $InCl_3$ [20]. An additional, smaller, pair of components occurs with the Cl $2p_{3/2}$ peak at 200.37 eV, attributed to organochloride contamination, as intentionally-prepared organochloride compounds display photoemission at a similar binding energy [21, 22].

The variation of the relative intensity of the $InCl_3$ component in the In $3d_{5/2}$ region is shown in figures 3, 4 and table 2 for sample A (as sample B contained negligible Cl, no change was observed after annealing). After annealing at 150 °C only a small reduction in the relative $InCl_3$ contribution is observed, accelerating as the annealing temperature is increased until 300 °C where the $InCl_3$ contribution is completely lost. The In_2O_3 component is unchanged, retaining the same ratio with the InSb component after all annealing processes.

Further evidence for the evolution of the surface of sample A as a function of annealing temperature was gathered from the Cl 2p region, as shown in figure 5. Here we see the total chlorine reducing with annealing temperature, with the chlorine loss accelerating rapidly above 150 °C until it is completely removed at 300 °C. Table 3 summarizes the changes in the total atomic percentages of each component present on the surface during the annealing process, further proving the removal of the $InCl_3$ layer with increasing annealing temperature.

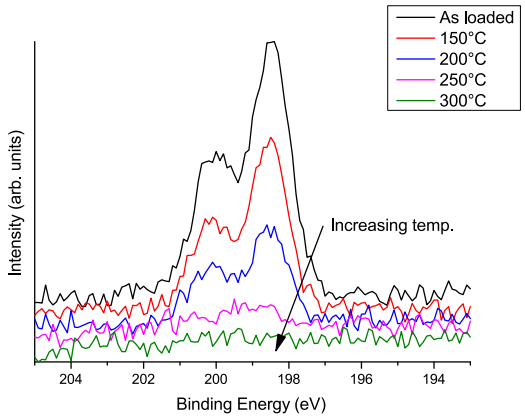

Figure 5. XPS data for the Cl 2p region of sample A. The as-received spectrum is shown in black (top), with spectra after a series of annealing steps shown in colour (below).

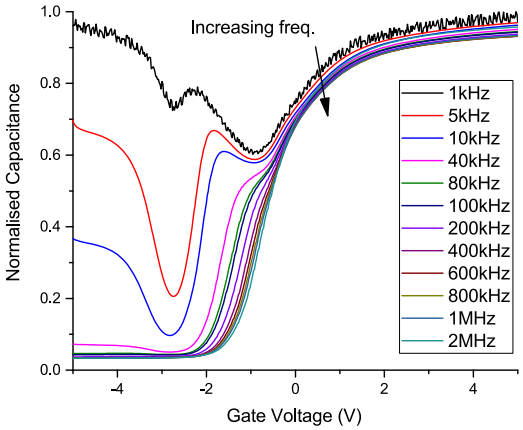

Figure 6. Typical multifrequency *C–V* response, taken for the HCl-water process and a deposition temperature of 200 °C.

Table 3. Variation in the In 3d and Cl 2p component atomic concentrations (as a percentage of the total In 3d and Cl 2p photoemission) in the near-surface region of sample A as a function of annealing temperature. Values accurate to ±2%.

Component	As-loaded	150 °C	200 °C	250 °C	300 °C
In–Sb	40.7	44.4	47.3	51.9	54.8
In–O	33.6	36.6	39.0	42.8	45.2
In–Cl	5.3	5.3	4.6	2.5	<0.1
Cl–In	18.8	13.3	7.9	2.9	<0.1
Cl-Contam.	1.6	0.4	1.1	<0.1	<0.1

To verify the time-dependency of the desorption of $InCl_3$, an additional InSb sample was prepared with the same HCl–IPA treatment as sample A and transferred to an Omicron Multiprobe instrument equipped with a Sphera hemispherical analyser in a similar manner to samples A and B. XPS spectra were taken as-received (and confirmed to be consistent with sample A) and the temperature of the sample was then raised to 250 °C, over 30 min with a ramp rate of approximately 7.7 °C min^{-1}. Once the sample had reached 250 °C, snapshot XPS spectra were taken to quantify the remaining Cl 2p emission and the In–Cl component in the In 3d spectrum. Within 5 min, the Cl 2p emission had dropped below the detection limit of the instrument.

Evidently exposure to higher temperatures accelerates the desorption of $InCl_3$ from the surface and thus MOSCAP structures were fabricated in order to investigate the effects of forming this $InCl_3$ layer.

4. Experimental methodology (*C–V*)

Three 2″ (~50 mm) wafers of InSb without intentional doping but with a carrier concentration of approximately 1×10^{14} cm^{-3} n-type (taken from the manufacturer's certificate of conformance) were cleaved in half, producing six samples of which five were used. Two samples received the same HCl–IPA treatment as sample A, two received the same HCl-water treatment as sample B and a control sample received no treatment. The samples were loaded into an Oxford Instruments OpAL ALD reactor promptly, with approximately 2 min exposure time in ambient air after removal from the rinse solution and before the ALD reactor was sealed and evacuated. Two samples, one for each wet treatment, and the control underwent deposition of 10 nm of Al_2O_3 at 200 °C as an Al-first process, with a carrier Ar flow of 100 sccm, a trimethylaluminium dose/purge time of 0.03/3 s and a water dose/purge time of 0.02/3 s. The relatively high oxide thickness was chosen for reliability, as the immaturity of the material system and lack of an ideal surface functionalisation for ALD prevent aggressive scaling of gate dielectrics without also impacting on yield and leakage current. The other two samples underwent the same process at the higher temperature of 250 °C. Following oxide deposition, the samples were degreased using acetone and isopropanol and 1 μm of Al metal was deposited in an SVS electron beam evaporator to serve as a gate contact. The gate metal was pattered using AZ 9260 photoresist as a mask and Microposit MF-319 photoresist developer (dilute tetra-methyammonium hydroxide) as an etchant. Post-deposition annealing was not performed, as no process has yet been demonstrated for the InSb-dielectric system below the non-congruent temperature of InSb [23]. The samples were diced for characterisation and characterised at a temperature of 80 K using a Leybold RDK 10-320 cryostat with a HP 4145 parameter analyser for *I–V* measurements and an Agilent E4980A LCR metre for *C–V* measurements, at frequencies between 1 kHz and 2 MHz. A typical *C–V* response is shown in figure 6.

During fabrication, it was observed that the surface wetting properties differed between the two wet treatments. The HCl–IPA solution and IPA rinse produced a surface with high wettability, consistent with a hydrophilic behaviour, whereas the HCl-water-treated surface displayed low wettability and was hydrophobic. For the HCl-water process, the sample surface repelled the etch and rinse solutions, accelerating their removal and potentially depositing particulates on the surface. For the HCl–IPA process, the sample surface retained the etch and rinse solutions until blown dry, thereby allowing particulates to be blown to the sample edge. For each process, four dies were prepared and 9 devices characterised per die, giving between 32 and 36 valid devices per process after wire bond failures were

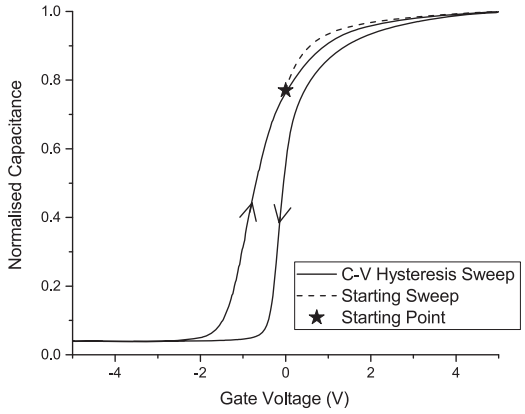

Figure 7. Typical bidirectional *C–V* response, taken at 2 MHz for the HCl-water process and a deposition temperature of 200 °C. The initial zero-bias measurement, before electrical stimulation, is shown by the star symbol and the initial sweep from the zero-bias point to +5 V is shown by the dashed line.

excluded. The HCl-water process displayed an overall yield poorer than the HCl–IPA process and also showed greater variability between repeating 10.9 × 9.2 mm device fields, with some fields matching the overall yield of the HCl–IPA process.

The interface-trapped charge density (D_{it}) was extracted using the Terman, high-low and conductance methods. Simulated *C–V* responses were generated following Engel-Herbert *et al* [24] and oxide capacitance was extracted from the measured accumulation capacitance using a correction factor from the simulated response. The simulated *C–V* response was also used to generate a flatband capacitance (C_{FB}) value, to enable the extraction of flatband voltage (V_{FB}, a measure of fixed charge in the system) from the high-frequency *C–V* response. In the *C–V* measurement, the DC voltage was swept from −5 to +5 V, with reverse sweeps performed at low and high frequency (5 kHz and 2 MHz), enabling D_{it} and V_{FB} to be extracted for both sweep directions on many samples, as well as hysteresis voltage at C_{FB} (V_H, a measure of oxide-trapped 'slow' or 'border' charge). A typical *C–V* hysteresis response is shown in figure 7, with the initial zero-bias measurement and *C–V* sweep from this point to +5 V also shown. As the starting point lies on the forward sweep (−5 to +5 V), V_{FB} has been extracted for the forward sweep direction.

After removing outliers, the distributions overlapped significantly and statistical hypothesis testing was necessary to extract significant trends. Distribution data for D_{it}, V_{FB} and V_H for all fabrication processes are shown in figures 8–10 respectively, with box plots showing the median, interquartile range and range. These plots illustrate that the data do not conform to the normal (Gaussian) distribution and, as such, a nonparametric test was chosen. While the Wilcoxon test is a well-known nonparametric test, it does not control for multiple testing, rendering it unsuitable for this application, as treatments must be compared to each other as well as the control. The Steel-Dwass test is both nonparametric and controls for multiple testing, enabling pairwise comparison of all data sets. A confidence interval of 95%, $\alpha = 0.05$ was used for all samples and mean values are provided in table 4.

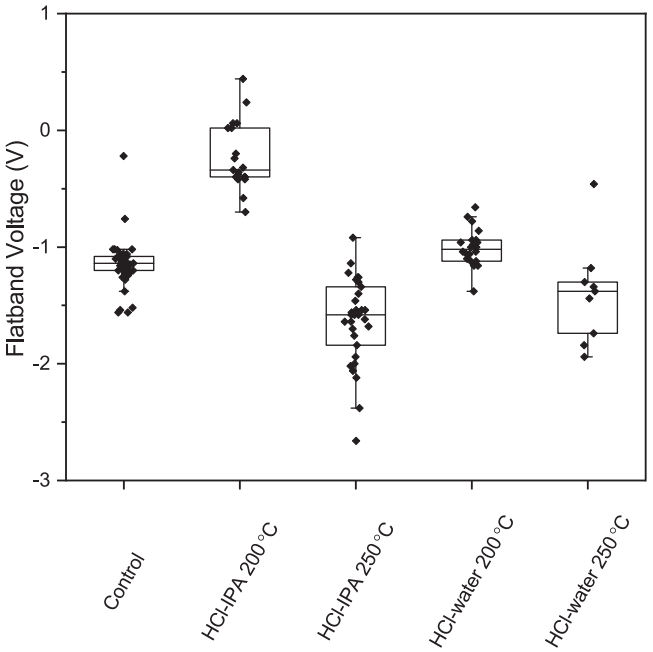

Figure 8. Distributions and variability of V_{FB} for the different fabrication processes. Box plots are shown for illustrative purposes only and statistical hypothesis testing was applied independently.

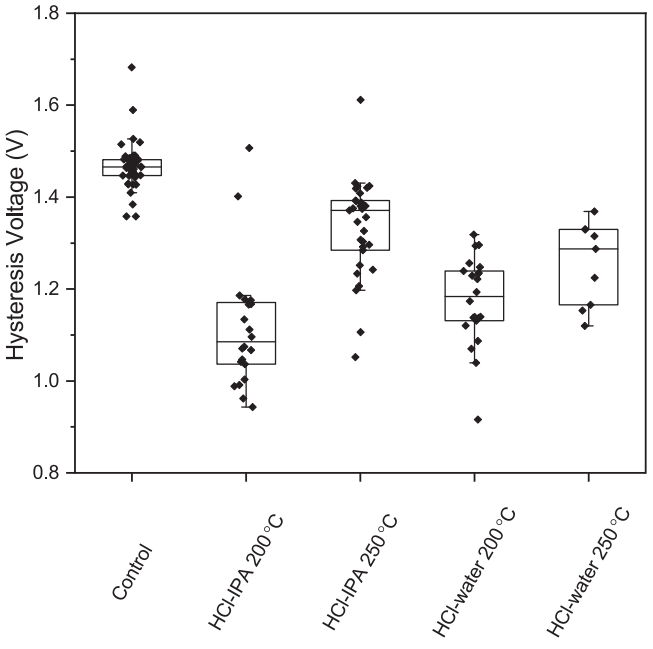

Figure 9. Distributions and variability of absolute V_H for the different fabrication processes. Box plots are shown for illustrative purposes only and statistical hypothesis testing was applied independently.

5. Results and analysis (*C–V*)

When comparing samples, only the HCl–IPA process with a deposition temperature of 200 °C includes a substantial $InCl_3$ interfacial layer, as XPS shows that it is either not formed (as in the HCl-water process) or is significantly desorbed (as with

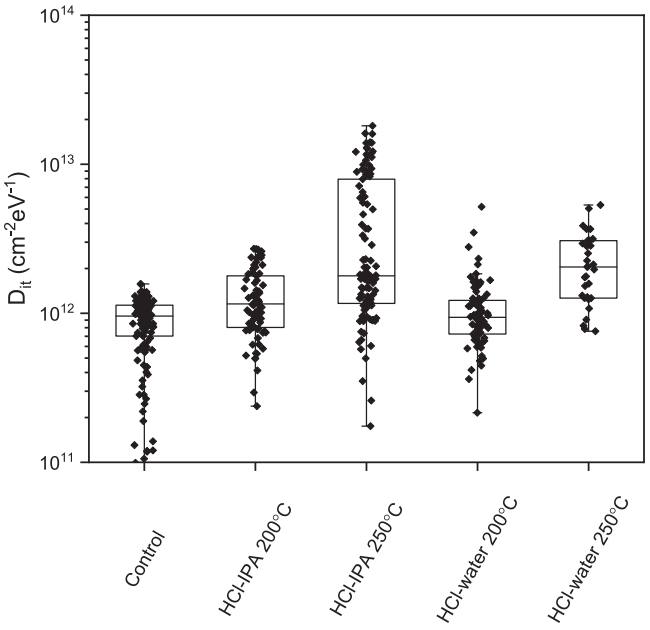

Figure 10. Distributions and variability of minimum D_{it} for the different fabrication processes. Box plots are shown for illustrative purposes only and statistical hypothesis testing was applied independently.

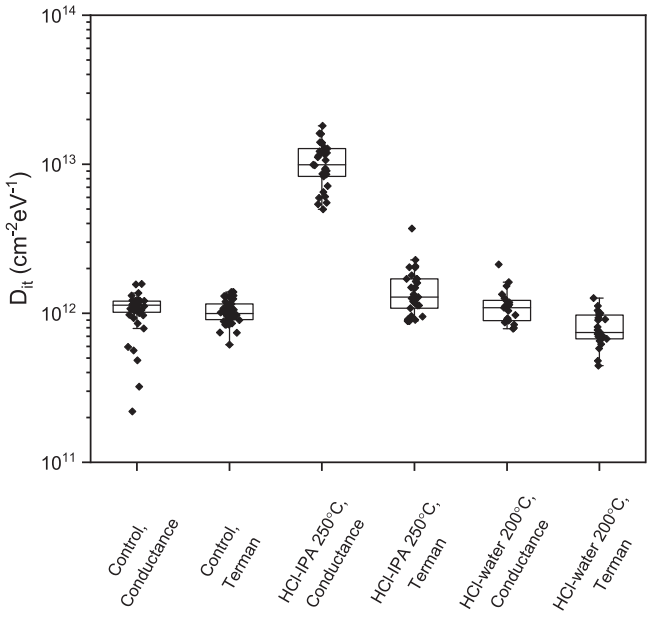

Figure 11. Distributions and variability of minimum D_{it} for the different fabrication processes and D_{it} extraction techniques. Box plots are shown for illustrative purposes only and statistical hypothesis testing was applied independently.

Table 4. Mean average values of D_{it}, V_{FB} and V_H for the different fabrication processes.

Process	D_{it} ($cm^{-2}\,eV^{-1}$)	V_{FB} (V)	V_H (V)
Control	8.7×10^{11}	−1.0	1.4
HCl–IPA 200 °C	1.3×10^{12}	−0.2	1.1
HCl–IPA 250 °C	4.3×10^{12}	−1.6	1.3
HCl-water 200 °C	1.0×10^{12}	−1.0	1.2
HCl-water 250 °C	2.3×10^{12}	−1.4	1.3

250 °C deposition temperature) for other samples. The HCl–IPA process at 200 °C shows a large positive shift in V_{FB} relative to the control (+0.79 V), whereas the HCl-water process at 200 °C showed no significant shift and the 250 °C processes showed negative shifts (−0.38 and −0.61 V) with no statistically significant difference between the HCl–IPA and HCl-water cleaning processes. The change to V_{FB} (and other figures of merit, discussed below) for a deposition temperature of 250 °C is likely due to the temperature sensitivity and degradation of the substrate material: InSb has a low melting point of 527 °C and can undergo decomposition at temperatures of 300 °C and potentially lower. Figure 8 shows the V_{FB} distributions for the different fabrication processes.

InSb MOSCAP devices have shown high hysteresis in previous publication [25] and similar results have been reproduced here, with >0.1 V of hysteresis per volt of the *C*–*V* sweep. However, all cleaning processes resulted in a decrease in hysteresis compared to the control sample, with the best results obtained with a lower deposition temperature of 200 °C and with no statistically significant difference between the cleaning processes. These results show evidence for reduction of 'slow' trap states, which impact device performance alongside 'fast' states characterised by D_{it}. Figure 9 shows the distributions of absolute V_H for the different fabrication processes.

The D_{it} showed no statistically significant improvement on the control sample, with an average minimum D_{it} of $8.71 \times 10^{11}\,cm^{-2}\,eV^{-1}$ (see figure 10). Although both 200 °C processes resulted in a small D_{it} increase relative to the control, the data variability is great enough that this result was found not to be statistically significant when tested. The 250 °C process, however, resulted in a significant increase in D_{it} for both cleaning processes, with a larger increase for the HCl–IPA process (to a D_{it} of $4.34 \times 10^{12}\,cm^{-2}\,eV^{-1}$) than for the HCl-water process (to a D_{it} of $2.25 \times 10^{12}\,cm^{-2}\,eV^{-1}$). This indicates that, although the $InCl_3$ interfacial layer can shift V_{FB} without affecting D_{it}, desorbing the $InCl_3$ layer will reverse the V_{FB} shift and increase D_{it}. Although the different D_{it} extraction processes showed the same trends, not all methods are equally sensitive to changes in fabrication process. The conductance method, in particular, showed a larger D_{it} increase for the HCl–IPA 250 °C process than the Terman and high-low methods, as shown in figure 11.

The critical difference between the HCl–IPA and HCl-water processes for a deposition temperature of 200 °C is the change in V_{FB}. This suggests that only fixed charge is introduced, without affecting D_{it} or 'slow' hysteresis charge and presents the opportunity to manipulate V_{FB} of MOSCAPs and, by extension, the threshold voltage of MOS transistor structures and the depletion/accumulation of passivation in other device structures, without impacting other figures of merit. The shift is substantial enough to move a MOS transistor threshold voltage from a depletion-mode device to an enhancement-mode device and may

offer a promising route to fabricate both types of devices using similar fabrication processes.

6. Conclusions

In summary, we have investigated the role of HCl treatments on InSb surfaces and interfaces with Al_2O_3 deposited by ALD. A surface layer of $InCl_3$ has been found to form when treated with HCl diluted in and rinsed with IPA but not for HCl diluted in and rinsed with DI water. The interfacial layer of $InCl_3$ has been associated with a flatband voltage shift of +0.79 V when processed at 200 °C but the $InCl_3$ layer is desorbed for a deposition temperature of 250 °C, causing the flatband voltage change to reverse. A lower deposition temperature of 200 °C resulted in lower D_{it} and hysteresis, with no statistically significant differences between the cleaning processes other than the shift in flatband voltage. This shift offers a promising route to manipulate the threshold voltage of MOS transistor structures and may allow enhancement-mode and depletion-mode devices to be fabricated in parallel, with otherwise identical fabrication processes.

Acknowledgments

This work was financed by EPSRC Engineering Fellowships for Growth: Narrow Band-gap Semiconductors for Integrated Sensing and Communications, grant number EP/M002411/1. The authors would additionally like to thank Ms Corinne Maltby and Mr Frank Courtney for support with device fabrication and wire bonding and Dr Vishal Shah and Dr Alan Burton for support with cryogenic electrical characterisation.

ORCID iDs

Oliver J Vavasour https://orcid.org/0000-0002-0919-9648

References

[1] Krier A 2007 *Mid-Infrared Semiconductor Optoelectronics* vol 118 (Berlin: Springer)
[2] Rogalski A, Martyniuk P and Kopytko M 2017 InAs/GaSb type-II superlattice infrared detectors: future prospect. *Appl. Phys. Rev.* **4** 21
[3] Nash G R, Forman H L, Smith S J, Robinson P B, Buckle L, Coomber S D, Emeny M T, Gordon N T and Ashley T 2009 Mid-infrared $Al_xIn_{1-x}Sb$ light-emitting diodes and photodiodes for hydrocarbon sensing. *IEEE Sens. J.* **9** 1240–3
[4] Gas Sensing Solutions 2017 Cozir ambient air CO_2 sensor https://gassensing.co.uk/products/ambient-air-sensors/cozir-ambient-air-co2-sensor/ (Accessed: 14 March 2018)
[5] del Alamo J A 2011 Nanometre-scale electronics with III–V compound semiconductors *Nature* **479** 317–23
[6] Ashley T *et al* 2007 Heterogeneous insb quantum well transistors on silicon for ultra-high speed, low power logic applications *Electron. Lett.* **43** 777–9
[7] Levinshtein M E, Rumyantsev S L and Shur M S 1996 *Handbook Series on Semiconductor Parameters* (Singapore: World Scientific)
[8] Vurgaftman I, Meyer J R and Ram-Mohan L R 2001 Band parameters for III–V compound semiconductors and their alloys *J. Appl. Phys.* **89** 5815
[9] Tereshchenko O E 2006 Structure and composition of chemically prepared and vacuum annealed InSb(001) surfaces *Appl. Surf. Sci.* **252** 7684–90
[10] Trinh H D, Nguyen M T, Lin Y C, Van Duong Q, Nguyen H Q and Chang E Y 2013 Band alignment parameters of Al_2O_3/insb metal-oxide-semiconductor structure and their modification with oxide deposition temperatures *Appl. Phys. Express* **6** 061202
[11] Trinh H-D, Chang E Y, Wong Y-Y, Yu C-C, Chang C-Y, Lin Y-C, Nguyen H-Q and Tran B-T 2010 Effects of wet chemical and trimethyl aluminum treatments on the interface properties in atomic layer deposition of Al_2O_3 on inas *Japan. J. Appl. Phys.* **49** 111201
[12] Chobpattana V, Son J, Law J J M, Engel-Herbert R, Huang C Y and Stemmer S 2013 Nitrogen-passivated dielectric/ingaas interfaces with sub-nm equivalent oxide thickness and low interface trap densities *Appl. Phys. Lett.* **102** 3
[13] Luc Q H, Do H B, Ha M T H, Hu C C, Lin Y C and Chang E Y 2015 Plasma enhanced atomic layer deposition passivated HfO_2/AlN/ $IN_{0.53}GA_{0.47}$ As moscaps with sub-nanometer equivalent oxide thickness and low interface trap density *IEEE Electron Device Lett.* **36** 1277–80
[14] Koh D, Shin S H, Ahn J, Sonde S, Kwon H M, Orzali T, Kim D H, Kim T W and Banerjee S K 2015 Damage free ar ion plasma surface treatment on $In_{0.53}GA_{0.47}$ As-on-silicon metal-oxide-semiconductor device *Appl. Phys. Lett.* **107** 3
[15] Iwasaki H, Mizokawa Y, Nishitani R and Nakamura S 1979 X-ray photoemission study of the initial oxidation of the cleaved (110) surfaces of gaas, gap and insb *Surf. Sci.* **86** 811–8
[16] Vasquez R P and Grunthaner F J 1981 Chemical composition of the SiO_2-InSb interface as determined by x-ray photoelectron spectroscopy *J. Appl. Phys.* **52** 3509–14
[17] Rastogi A and Reddy K V 1995 Growth of dielectric layers on the insb surface *Thin Solid Films* **270** 616–20
[18] Faur M, Faur M, Jayne D T, Goradia M and Goradia C 1990 XPS investigation of anodic oxides grown on p-type inp *Surf. Interface Anal.* **15** 641–50
[19] Clark D T, Fok T, Roberts G G and Sykes R W 1980 An investigation by electron spectroscopy for chemical analysis of chemical treatments of the (100) surface of n-type inp epitaxial layers for langmuir film deposition *Thin Solid Films* **70** 261–83
[20] Freeland B H, Habeeb J J and Tuck D G 1977 Cordination compounds of indium: XXXIII. X-ray photoelectron spectroscopy of neutral and anionic indium halide species *Can. J. Chem.-Rev. Can. Chim.* **55** 1527–32
[21] Zhou X L, Solymosi F, Blass P M, Cannon K C and White J M 1989 Interactions of methyl halides (CL, BR and I) with Ag(111) *Surf. Sci.* **219** 294–316
[22] Ohta T, Yamada M and Kuroda H 1974 X-ray photoelectron spectroscopy of p-benzoquinone, hydroquinone and their halogen-substituted derivatives *Bull. Chem. Soc. Japan* **47** 1158–61
[23] Trinh H D *et al* 2013 Electrical characteristics of AL_2O_3/InSb moscaps and the effect of postdeposition annealing temperatures *IEEE Trans. Electron Devices* **60** 1555–60
[24] Engel-Herbert R, Hwang Y and Stemmer S 2010 Comparison of methods to quantify interface trap densities at dielectric/III–V semiconductor interfaces *J. Appl. Phys.* **108** 124101
[25] Kadoda A, Iwasugi T, Nakatani K, Nakayama K, Mori M, Maezawa K, Miyazaki E and Mizutani T 2012 Characterization of AL_2O_3/InSb/Si mos diodes having various insb thicknesses grown on Si(111) substrates *Semicond. Sci. Technol.* **27** 6